Study of the electric field in a diffuse nanosecond positive ionization wave generated in a pin-to-plane geometry in atmospheric pressure air

Anne Bourdon, François Péchereau, Fabien Tholin, Zdenek Bonaventura

Study of the electric field in a diffuse nanosecond positive ionization wave generated in a pin-to-planegeometry in atmospheric pressure air

Study of the electric field in a diffuse nanosecond positive ionization wave generated in a pin-to-plane geometry in atmospheric pressure air

Anne Bourdon[1], François Péchereau[2], Fabien Tholin[2] and Zdenek Bonaventura [3]

[1] LPP, CNRS, École Polytechnique, Sorbonne Université, IP Paris, route de Saclay, 91128 Palaiseau, France

[2] ONERA, 6, chemin de la Vauve aux Granges, 91123 Palaiseau, France

[3] Faculty of Science, Masaryk University, Brno, Czech Republic

E-mail: anne.bourdon@lpp.polytechnique.fr

18 September 2020

Abstract. The dynamics of a nanosecond positive ionization front generated in a pin-to-plane geometry in atmospheric pressure air is simulated using a 2D axisymmetric drift-diffusion fluid model. For a 16 mm gap and a sharp pin electrode, the plateau of the applied voltage is varied between 40 and 60 kV and the rise time is varied between 0.5 and 1.5 ns or a DC voltage is applied. The discharge ignition time and the voltage at ignition are shown to depend mostly on the voltage rise time. The connection time, i.e. the time for the ionization wave to ignite, propagate and connect to the plane is shown to strongly depend on both the values of the voltage plateau and rise time. For all cases, the discharge has a conical shape with a maximal radius of about 8 mm as it connects to the grounded plane. The average propagation velocity of the ionization front is found to vary in the range 3.1 to 8.5 mm ns^{-1}. These values are in rather good agreement with experiments. Temporal evolutions of the electric field are recorded on the symmetry axis at different positions in the gap. At each location, an increase and decrease of the electric field is observed as the ionization front, propagating from the pin to the plane, passes the studied point, in accordance with experimental observations. Finally, for a voltage plateau of 55 kV and a rise time of 0.5 ns, a temporal sampling of 100 ps is shown to be sufficient to capture the dynamics of the electric field during the ionization front propagation when it passes close to the middle of the gap. Conversely, a temporal sampling of 10 ps is required when the ionization wave is close to both electrodes, or during the fast redistribution of the electric field after the connection of the ionization front at the cathode.

Keywords: nanosecond discharge in air at atmospheric pressure, streamer discharge, fluid simulation

Submitted to: *J. Phys. D: Appl. Phys.*

1. Introduction

Nanosecond discharges in air at atmospheric pressure are of significant interest both from a fundamental viewpoint and for engineering applications. However the detailed study of these discharges, even in a simple point-to-plane geometry, is difficult both experimentally and numerically as they may easily branch and then have complex 3D structures (Tardiveau et al.; 2002; Pancheshnyi et al.; 2005; Briels et al.; 2008; Nijdam; 2011; Teunissen and Ebert; 2016). In the 1970s, Marode (1975a,b) proposed a set-up to generate stable and repetitive 2D axisymmetric discharges in air at atmospheric pressure and room temperature. This set-up consists of a point-to-plane geometry with a gap of about 1 cm and a low positive DC voltage of up to 20 kV applied to the point electrode. In these conditions, at a repetition frequency of a few kHz, a positive ionization wave usually called positive streamer is ignited close to the point electrode and propagates in the gap towards the plane (Marode; 1975a,b; Dubois et al.; 2007; Eichwald et al.; 2008). The characteristics of the positive ionization front for gaps of about 1 cm and for applied voltages of up to 20 kV have been also extensively studied numerically (Marode; 1975b; Babaeva and Naidis; 1996; Kulikovsky; 1998; Pancheshnyi et al.; 2000; Dubois et al.; 2007; Eichwald et al.; 2008; Celestin et al.; 2009; Marode et al.; 2009). During the propagation, the maximum electric field in the ionization front is in the range of 100 to 150 kV cm^{-1} and the radius of the discharge channel behind the front is rather constant and is of a few 100s μm. The average propagation velocity of the ionization front is about 0.1–0.2 mm ns^{-1}. After the arrival at the cathode, there is a very fast redistribution of electric field and electrical charges in the gap, known as a return stroke (Sigmond; 1984) which propagates very rapidly in the gap from the cathode towards the anode. This return stroke is very difficult to observe in air at atmospheric pressure due to its fast dynamics and very low optical emission. Conversely, after the return stroke, light emission is clearly observed close to the point anode and its extension towards the plane is called secondary streamer propagation (Marode; 1975a; Sigmond; 1984; Eichwald et al.; 2008). The development of the secondary streamer relates rather to a plasma structuration than to a real streamer mechanism. The field in a secondary streamer is about 30 kV cm^{-1} and then is much lower than that in the first streamer.
To study positive streamer characteristics at higher voltages, pulsed voltages have been used (Yi and Williams; 2002; Ono and Oda; 2003; Tardiveau et al.; 2002; Pancheshnyi et al.; 2005; Briels et al.; 2006, 2008; Nijdam; 2011; Komuro et al.; 2013; Ono and Komuro; 2019). Despite the complexity induced by discharge branching, Briels et al. (2006, 2008) have carried out detailed experimental studies on the influence of the peak applied voltage and the voltage rise time on positive streamer characteristics in a point-to-pane geometry in air at atmospheric pressure with pulsed applied voltages. In Briels et al. (2006), for a gap of 40 or 80 mm, and peak applied voltages between 40 and 60 kV, it is observed that streamer diameters grow with the increase of the applied voltage between 0.2 and 2.5 mm and the streamer velocity increases with the diameter, ranging from 0.07 to 1.5 mm ns^{-1}. With voltage rise time varying between 23 and 60

ns, it is also shown that as the voltage time rate (in kV ns^{-1}) is increased, the velocity and diameter of the primary streamer increases in atmospheric-pressure air. In Briels et al. (2008), in a 4 cm gap, with an applied voltage of 96kV and a rise time of 15 ns (i.e. voltage time rate of 6.4 kV ns^{-1}), positive streamers attain diameters of 3 mm and velocities of 4 mm ns^{-1}. Using a array of needle electrodes, Ono and Oda (2003); Komuro et al. (2013); Ono and Komuro (2019) have obtained non branching mono-filament-like primary and secondary streamers in air at atmospheric pressure in a 13 mm with pulsed applied voltages. In Komuro et al. (2013), for peak applied voltages in the range 18 to 25 kV, it is shown in 2D fluid simulations that as the voltage time rate increasing from 0.11 kV ns^{-1} to 0.52 kV ns^{-1}, there is an increase of the diameter of the streamer channel and of the propagation velocity of the primary streamer from 0.49 to 0.69 mm ns^{-1}. Same trends are observed in experiments. The simulated reduced electric field of the primary streamer head is shown to remain constant and not to depend on the voltage time rate.

Recently, attention has been attracted to 2D axisymmetric diffuse discharges with radii of several millimeters produced at high overvoltages applied with subnanosecond voltage fronts. In a recent review, Naidis et al. (2018) present the results of experimental and numerical studies of subnanosecond diffuse discharge formation in various gases for different polarities, geometries and applied voltages. For air at atmospheric pressure in point-to-plane geometries with gaps of about 1 cm, so far, there is still only a small number of experimental and numerical studies on diffuse discharges for positive voltages (in the range 30 to 250 kV) applied at a point electrode with a nanosecond rise time (i.e. voltage time rate in the range 30-250 kV ns^{-1}) (Naidis et al.; 2018; Tardiveau et al.; 2008; Tardiveau et al.; 2009; Pechereau et al.; 2014; Babaeva and Naidis; 2016b; Babaeva and Naidis; 2016a; Marode et al.; 2016; Tardiveau et al.; 2016; Brisset et al.; 2019). In experiments, it is observed that after the discharge ignition in the high-field region at the vicinity of the point electrode, a large volume positive ionization wave propagates in the gap towards the grounded plane. As discussed in Naidis et al. (2018), the dynamics of most of the electrons in ionization fronts produced by high overvoltages applied with subnanosecond voltage fronts can be described using a classical 2D axisymmetric fluid approach. However, for these conditions, fast (runaway) electrons may be produced near the point electrode and could have an impact on the formation of x-rays, the gas preionization and the dynamics and structure of positive diffuse ionization fronts (Naidis et al.; 2018; Tarasenko; 2020). So far, comparison studies between experiments and 2D fluid simulations have been focused on discharge structure and average propagation velocity. In Pechereau et al. (2014), the dynamics of a nanosecond ionization wave in air at atmospheric pressure has been simulated for a point-to-plane geometry in conditions close to experiments with a pulsed applied voltage of 30 kV, a rise time of 2 ns and for a 1 cm gap. A good agreement between experimental and simulated optical emissions of the discharge has been obtained on : the conical discharge structure when the discharge connects with the plane cathode, the maximum discharge diameter of 8 mm, and on its average propagation velocity of 2.6 mm ns^{-1}. For a point to plane

geometry with a 1.5 cm gap and a positive voltage of 250 kV applied to the point electrode with a subnanosecond voltage front, a discharge radius of up to 1 cm and a propagation velocity in the range of 10 to 100 mm ns^{-1}, similar to experimental data, is simulated in Babaeva and Naidis (2016b). In Tardiveau et al. (2016), the discharge characteristics for a pulsed applied voltage of 50 kV with a rise time of 2 ns in a point-to-plane geometry with a 1 cm gap have been simulated and compared to experiments. A good agreement is observed on the global structure of the light emission of the diffuse discharge but the computed discharge current and the ionization front propagation velocity are smaller than in experiments. In Brisset et al. (2019), the discharge dynamics in a point-to-plane geometry with a 18 mm gap and the same applied voltage pulse as in experiments with a peak value of 85 kV and a rise time of 2 ns has been simulated. A good agreement between experiments and simulations is obtained at early times on the maximum electric field, on the position of this maximum and on the propagation velocity (about 2 mm ns^{-1}). Then in experiments, the propagation velocity increases during propagation and is about 10 mm ns^{-1} in average. In simulations, the calculated radial expansion of the discharge is smaller than in experiments and the average value of the propagation velocity is only of 4.5 mm ns^{-1}.

Very recently, to better understand the physics of positive diffuse ionization waves in point-to-plane geometry in air at atmospheric pressure, different diagnostics have been used to measure the time evolution of the electric field in several locations in the gap: in Brisset et al. (2019) using optical emission spectroscopy and the intensity ratio of two well-known transitions of molecular nitrogen and in Chng et al. (2019) using the recently developed Electric Field Induced Second Harmonic (E-FISH) diagnostic. Conditions studied in both works are close: positively pulsed high voltages (20 to 85 kV) with a rise time of 2–3 ns applied to a point anode with a radius of curvature of 50 to 100 μm in a point-to-plane geometry with an interelectrode gap of 10 to 18 mm. It is interesting to note that, no x-ray emission has been detected in the experimental set-up studied in Brisset (2019); Chng et al. (2019); Brisset et al. (2019). Even if there are several limitations to the applicability of the intensity-ratio method for the study of very transient phenomena, the achieved temporal resolution of electric field measurement is assumed to be 500 ps (Brisset et al.; 2019). For the E-FISH diagnostic, in Chng et al. (2019), the effective time resolution of measurements is estimated to be 150 ps. These recent measurements show a high electric field zone propagating towards the plane electrode (Brisset; 2019). Based on the single shot data with E-FISH diagnostic (Chng et al.; 2019), the maximum electric field in the ionization front is shown to be moderately influenced by the applied voltage and varies between 160 and 210 kV cm^{-1}. An electric field enhancement compared to the Laplacian field is measured ahead of the ionization front during its propagation. Behind the front, the electric field increases with the applied voltage and values of 20 kV cm^{-1} close to the breakdown field in air have been measured. The average propagation velocity of the ionization front varies between 6 to 10 mm ns^{-1} for applied voltages increasing from 65 to 85 kV (Brisset; 2019). When the ionization wave reaches the grounded electrode, the discharge transitions into a

conduction phase in which the potential is redistributed within the gap. The electric field increases again, but to lower values.

The objective of this work is to study the time evolution of the electric field in different points of the gap during the ignition, propagation and connection at the cathode of a pulsed nanosecond diffuse discharge in air at atmospheric pressure in a pin to plane geometry using fluid simulations and to compare with recent measurements (Brisset; 2019; Chng et al.; 2019). For atmospheric pressure studies, the geometry of electrodes and holders and the accurate knowledge of the location of grounded surfaces around the experimental set-up is of key importance for comparison between experiments and simulations (Xiong et al.; 2012). In this work, we use both a simplified geometry and voltage shape in comparison to experiments. Therefore the comparison will be only qualitative. In the simulations in Babaeva and Naidis (2016b); Babaeva and Naidis (2016a), a sphere electrode (radius of 2.5 to 5 mm) for a 1.5 cm gap is used. In the simulations in Marode et al. (2016); Tardiveau et al. (2016); Brisset et al. (2019), the gap is in the range of 1 to 1.8 cm. A parabolic point with a radius of curvature of 50 μm is used and a disc is put as a point holder at 1 cm from the tip. In Pechereau et al. (2014), for a 1 cm gap, the pin electrode is a rod of radius 50μm ended by a half sphere. In the present work, similarly as in Pechereau et al. (2014), we use a thin pin electrode with a simple shape. However a larger gap size and higher applied voltage values are used in comparison to Pechereau et al. (2014) to be closer to experimental conditions in Brisset (2019); Chng et al. (2019).

In section 2, we set out the pin-to-plane geometry and the 2D drift-diffusion fluid model used to simulate the nanosecond diffuse discharge in air at atmospheric pressure and room temperature. In section 3.1, we first present the simulation of the discharge dynamics of a diffuse nanosecond discharge for a reference condition. In sections 3.2 and 3.3, we study the influence of the value of the voltage plateau and the voltage rise time, respectively, on the discharge dynamics and characteristics : propagation velocity, maximal discharge radius and electric field on the discharge axis. Finally, in section 3.4, we analyze the time evolution of the electric field for several points in the gap of a diffuse nanosecond discharge and we compare with experiments.

2. Model formulation

The studied configuration is a simple pin-to-plane geometry with a positive voltage applied to the pin electrode set above the grounded plane. In this work, we use a classical 2D fluid model based on drift-diffusion equations for electrons, positive and negative ions (with subscripts 'e', 'p' and 'n' respectively) coupled with Poisson's equation in cylindrical coordinates (x, r) to simulate the dynamics of axisymmetric discharges in air at atmospheric pressure (Kulikovsky; 1997; Tholin; 2012; Pechereau; 2013) :

$$\frac{\partial n_{\mathrm{e}}}{\partial t} - \nabla \cdot (n_{\mathrm{e}} \mu_e \mathbf{E}) - \nabla \cdot (D_{\mathrm{e}} \nabla n_{\mathrm{e}}) = S_{\mathrm{ph}} + S_{\mathrm{e}}, \tag{1}$$

$$\frac{\partial n_{\rm p}}{\partial t} + \nabla \cdot (n_{\rm p}\mu_p \mathbf{E}) = S_{\rm ph} + S_{\rm p}, \tag{2}$$

$$\frac{\partial n_{\rm n}}{\partial t} - \nabla \cdot (n_{\rm n}\mu_n \mathbf{E}) = S_{\rm n}, \tag{3}$$

$$\varepsilon_0 \Delta V = -q_{\rm e}(n_{\rm p} - n_{\rm n} - n_{\rm e}), \quad \mathbf{E} = -\nabla V, \tag{4}$$

where n_i and μ_i are the density and the absolute value of the mobility of species i respectively, $D_{\rm e}$ is the diffusion coefficient of electrons, $\mathbf{E}$ is the electric field and V is the electric potential. As in Jánský et al. (2010), on the timescales of the discharge dynamics studied in this paper, the diffusion of ions is neglected. $q_{\rm e}$ is the absolute value of electron charge and ε_0 is the permittivity of free space. The following equations describe the source terms for electrons $S_{\rm e}$, positive ions $S_{\rm p}$ and negative ions $S_{\rm n}$:

$$S_e = (\alpha|W_e| - \eta|W_e| - \beta_{\rm ep} n_{\rm p})\, n_{\rm e}, \tag{5}$$

$$S_p = -(\beta_{\rm ep} n_{\rm e} + \beta_{\rm np} n_{\rm n})\, n_{\rm p} + \alpha|W_e| n_{\rm e}, \tag{6}$$

$$S_n = -\beta_{\rm np} n_{\rm p} n_{\rm n} + \eta|W_e| n_{\rm e}, \tag{7}$$

where $|W_e| = |\mu_e\ E|$ is the absolute value of the electron drift velocity, α and η stand for the ionization and attachment coefficients respectively. $\beta_{\rm ep}$ is the recombination rate coefficient between positive ions and electrons and $\beta_{\rm np}$ is the recombination rate coefficient between positive and negative ions. In this work we use the local field approximation. Then, transport coefficients and source terms of the model are assumed to be explicit functions of the local reduced electric field E/N, where E is the electric field magnitude and N = 2.45×10^{25} m^{-3} is the air neutral density, and are taken from Morrow and Lowke (1997). The $S_{\rm ph}$ term is the rate of electron-ion pair production due to photoionization in the gas volume and is modelled using (Bourdon et al.; 2007) with boundary conditions given in Liu et al. (2007).

The geometry of electrodes and boundary conditions for Poisson's equations are particularly important for the dynamics and structure of atmospheric pressure discharges. In this work, the pin electrode is a rod of radius 100 μm ended by a half sphere. The length of the pin electrode is 1 cm. The grounded plane ($x = 0$ cm) is located at 1.6 cm from the tip of the pin electrode. The radius of the plane is the same as the radial expansion of the simulation domain and is 7.52 cm. The computational domain is 2.6 cm $\times$ 7.52 cm with a Cartesian grid. In the axial direction, close to tip of the pin electrode (from $x = 1.3$ to 1.75 cm) a mesh size of 1 μm is used and then the mesh size is increased following a geometric progression up to 5 μm and is kept constant in the gas gap down to the cathode. From $x = 1.75$ cm to the upper boundary of the domain, the mesh size is increased from 1 μm following a geometric progression. In the radial direction, a mesh size of 1 μm is used from the axis of symmetry up to $r = 0.07$ cm and is then increased to 5 μm and is kept constant up to $r = 0.76$ cm and then the mesh follows a geometric progression until $r = 7.52$ cm. Finally the grid used is this work is $n_x \times n_r = 7252 \times 2400$. In the following, to present clearly the results,

we use 1D and 2D figures centered on a smaller domain of 1.8 cm × 0.8 cm.

In this work, we have taken into account simplified boundary conditions for continuity equations at the anode and cathode surfaces. On the cathode plane, Neumann boundary conditions are applied for all charged particle fluxes. At the pin anode, the fluxes directed outward the electrode are estimated using Neumann boundary conditions for electrons and set to zero for ions. For Poisson's equation, at the metallic pin electrode-air interfaces, the ghost-fluid method is used (Celestin et al.; 2009) with a Dirichlet boundary condition. The plane electrode is grounded. At other axial and radial boundaries (i.e. symmetry axis and the radial border of the computational domain) Neumann boundary conditions are used. Other characteristics of the simulations (numerical methods and time-step calculation, code parallelization and performance) are presented in detail in Pechereau (2013). As initial condition, a low uniform density of 10^4 cm^{-3} electrons and positive ions in air is considered, to be close to single pulse experiments.

In this work, we study the discharge ignition and dynamics for different rise times and values of the voltage plateau. Once the voltage plateau is reached, the voltage is kept constant to compare the time needed by the discharge to cross the interelectrode gap for different applied voltages. First, as a reference, in section 3.1, we study the discharge ignition and dynamics for a pulsed voltage with a rise time of 0.5 ns and a voltage plateau of 55 kV as shown on Figure 1. Then in section 3.2, for the same voltage rise time, we vary the value of the voltage plateau in the range of 40 to 60 kV. Then, for a voltage plateau of 55 kV, in section 3.3, the influence of the voltage rise time is studied by applying either a DC voltage or by increasing the rise time from 0.5 to 1.5 ns, as shown on Figure 1.

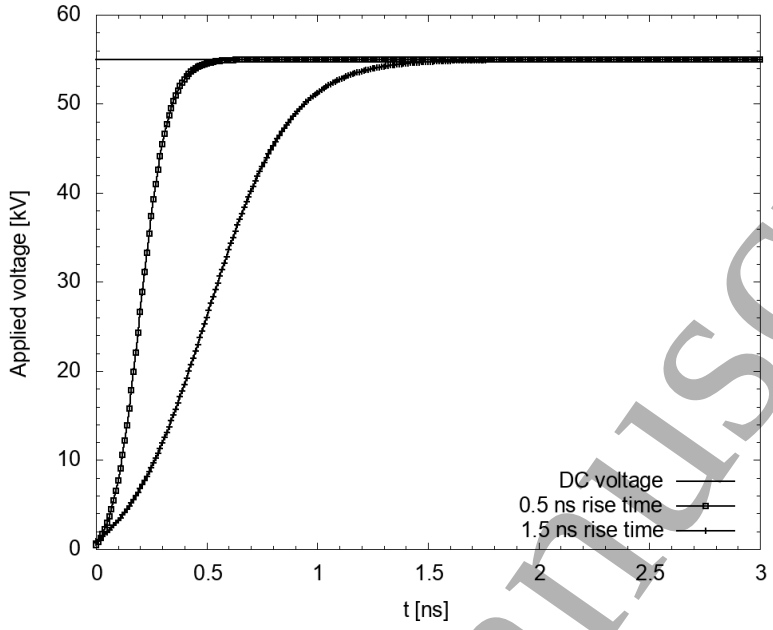

Figure 1. Different time evolutions of the applied voltage used in this work for a voltage plateau of 55 kV.

3. Results and discussion

3.1. Reference simulation: Discharge dynamics and characteristics for an applied voltage of 55 kV and a rise time of 0.5 ns

Figures 2 and 3 show the dynamics of the discharge for the reference applied voltage of 55 kV and a rise time of 0.5 ns. Figure 2 shows cross-sectional views of the absolute value of the electric field and electron density at $t = 0.5$, 1, 1.5, 2, 2.45 and 2.6 ns. As shown on Figure 2, the discharge is axisymmetric during its ignition, propagation and after the connection at the plane, with a maximum of electric field on the symmetry axis. Figure 3 shows profiles of electric field and electron density along the symmetry axis of the computational domain for the moments of time from $t = 0.2$ to $t = 2.6$ ns, with a timestep of 0.2 ns. We observe that the discharge ignites around the sharp pin electrode in the first 0.2 ns and starts propagating axially towards the cathode plane. Figure 2 shows that at $t = 0.5$ ns, at the start of the voltage plateau, the discharge has a spherical structure with a radius of about 3 mm. During the axial propagation of the discharge, its radius increases to about 8 mm. The discharge connects to the grounded plane at $t = 2.45$ ns, and has a conical shape as observed in experiments (Tardiveau et al.; 2008; Tardiveau et al.; 2009) and in simulations for shorter gap and lower voltage (Pechereau et al.; 2014). In experiments, a short voltage pulse is used to prevent the transition to a highly conductive spark discharge after the connection. In our simulations, there is a voltage plateau for $t > 0.5$ ns. As the study of the transition to the highly conductive spark discharge is out of the scope of this work, we have stopped

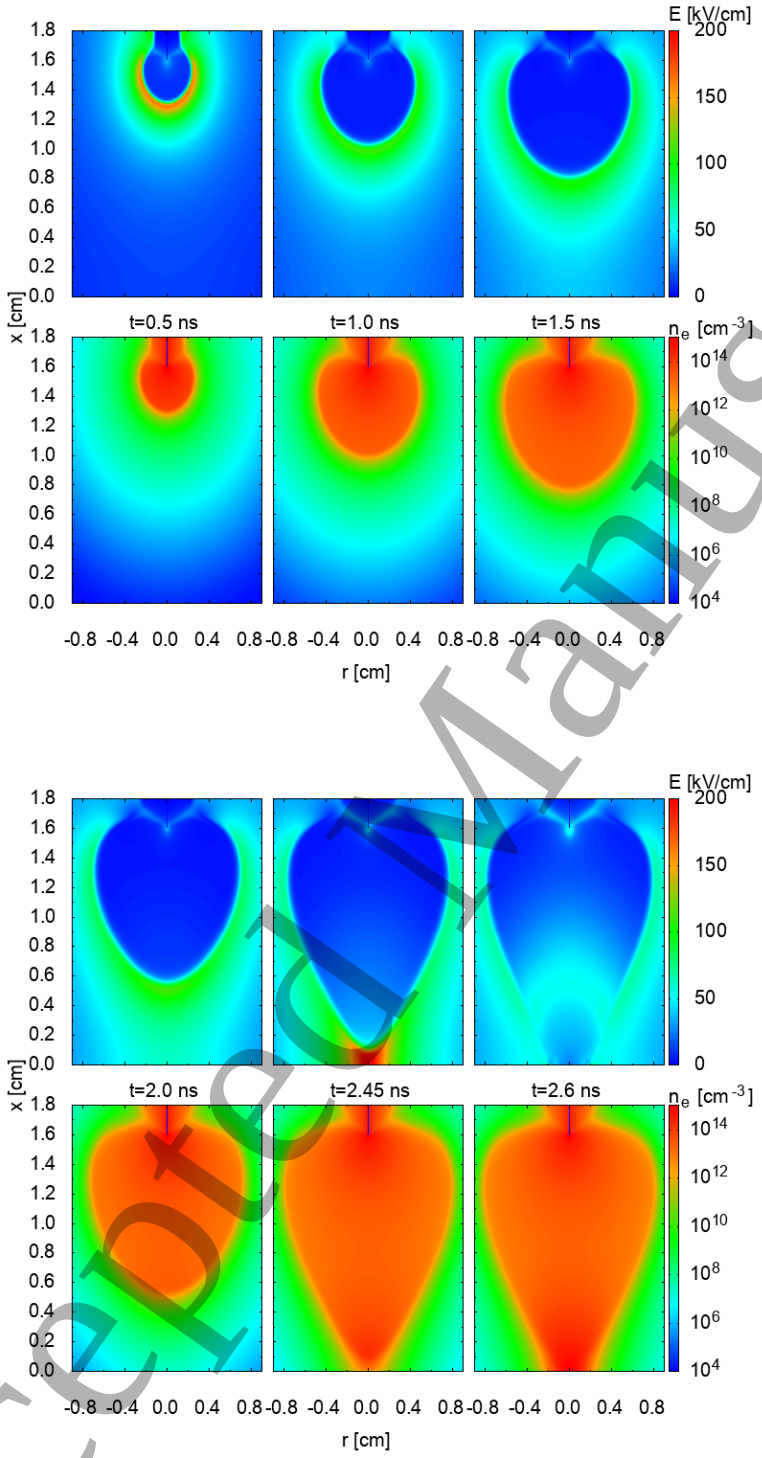

Figure 2. Dynamics of the discharge for an applied voltage of 55 kV and a rise time of 0.5 ns. Cross-sectional views of the absolute value of the electric field and electron density at $t = 0.5$, 1, 1.5, 2, 2.45 and 2.6 ns.

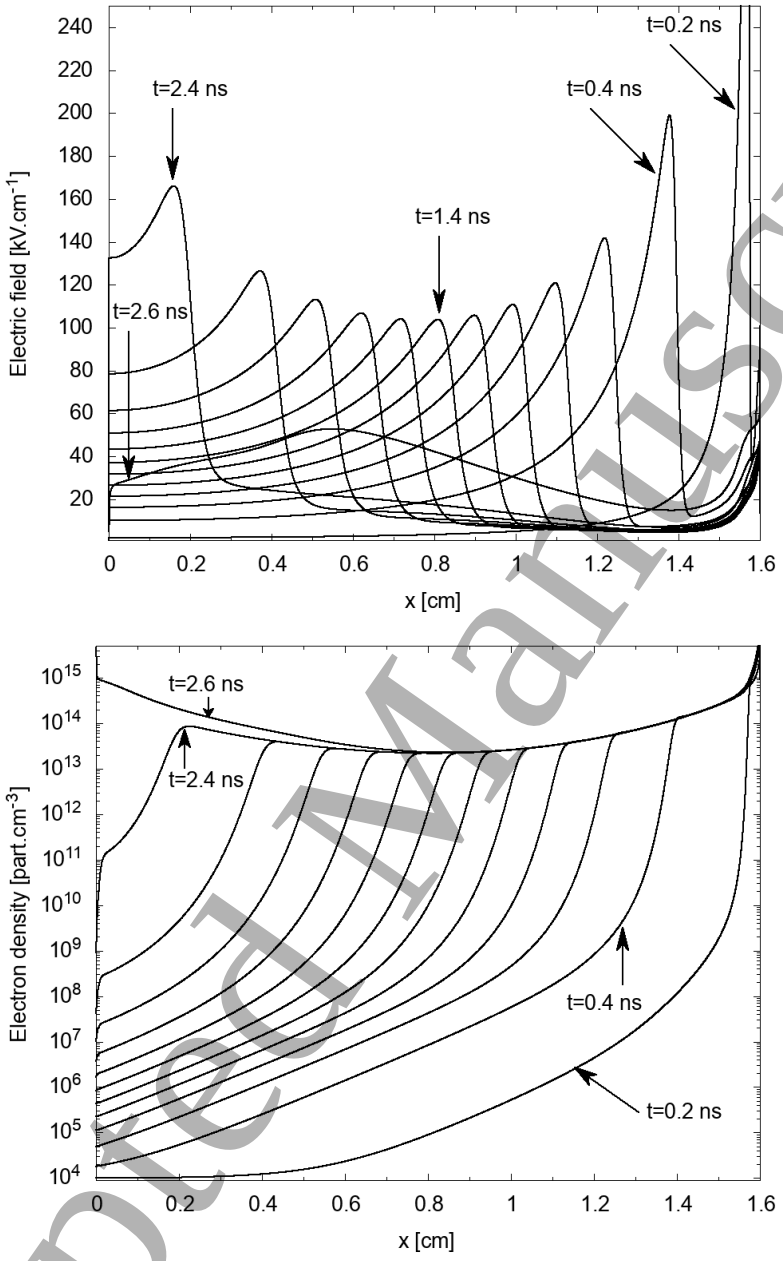

Figure 3. For an applied voltage of 55 kV and a rise time of 0.5 ns: profiles of electric field and electron density along the symmetry axis of the computational domain for the moments of time from t = 0.2 to t = 2.6 ns, with a timestep of 0.2 ns. The tip of the pin electrode is located at x=1.6 cm.

simulations at $t = 2.65$ ns just before the timestep starts decreasing sharply due to the increase of the electron density in the conductive channel.

Figure 3 shows that for $t \geq 0.4$ ns, $E_{x,max}$, the maximum of the electric field on the symmetry axis is less than 220 kV cm^{-1}. For, $t < 0.4$ ns higher values are obtained: more precisely, we have checked that $E_{x,max}$ is higher than 240 kV cm^{-1} from $t = 0.06$ ns to 0.32 ns and that $E_{x,max}$ reaches a maximal value at $t = 0.14$ ns of 870 kV cm^{-1}. According to Kunhardt et al. (1986), a fluid model is acceptable for an electric field up to 1000 Td $\simeq$ 250 kV cm^{-1} which is also the lower limit to accelerate electrons to runaway regime (Moss et al.; 2006). In the results obtained in this work, it is interesting to note that values of electric field higher than 250 kV cm^{-1} are obtained only for a very short duration. Then, as stated in Naidis et al. (2018), as the residence times of electrons in these regions are very short, only a very small part of the electrons may reach runaway energies. In this work, as a first step, we neglect the influence of these transient high field values on the dynamics of discharge propagation in the gap. For $t \geq 0.4$ ns, as the discharge propagates axially, $E_{x,max}$ decreases down to about 104 kV cm^{-1} when the ionization front is close to the middle of the gap at $x = 0.8$ cm. Then $E_{x,max}$ starts increasing again as the ionization front gets closer to the plane cathode. It is interesting to note that during the ionization front propagation, behind the discharge front, the electric field is low in the discharge channel, as expected, but increases as the discharge propagates, to values higher than 20 kV cm^{-1}. Close to the tip of the pin electrode, for $t > 0.2$ ns and until the connection at the plane, the electric field remains in the range of 40–50 kV cm^{-1}. At $t = 2.45$ ns, when the discharge connects to the cathode plane, the maximum electric field at the cathode is of 215 kV cm^{-1}. Rapidly after the connection, there is a fast redistribution of electric field in the conductive channel, known as return stroke (Sigmond; 1984), with a return wave propagating from the grounded plane towards the anode as shown on Figure 2 at $t = 2.6$ ns. Figure 3 shows that the peak of electric field in the return wave is much more diffuse than in the first ionization wave with a maximal value of 53 kV cm^{-1}. At $t = 2.6$ ns, the maximal electric field in the gap is located at the tip of the pin anode with a value of 60 kV cm^{-1}. It is interesting to note that after the connection, the electric field is non uniform and is in many points of the gap higher than the breakdown field in air at atmospheric pressure. The dynamics of the redistribution of electric field in the gap after the connection at the cathode is studied in more detail in section 3.4.

Figure 3 shows that the electron density in the discharge channel behind the discharge front evolves during the front propagation and is not uniform axially. The minimal value of electron density in the channel is observed at $x = 0.8$ cm and is about 2×10^{13} cm^{-3}. For $x > 0.8$ cm and up to the tip of the pin, the electron density in the channel increases smoothly and we note that values higher than 10^{15} cm^{-3} are obtained in the last 200 μm close to the anode tip. For $x < 0.8$ cm, as the discharge front approaches the cathode, the electron density behind the discharge front increases again. After the connection, a conductive channel is formed between both electrodes, with a minimal density of 2×10^{13} cm^{-3} in the gap and values higher than 10^{15} cm^{-3} close to both electrodes as

shown on Figures 2 and 3 at $t = 2.6$ ns.

3.2. Influence of the value of the voltage plateau between 40 and 60 kV *for a voltage rise time of 0.5 ns on the discharge dynamics and characteristics*

In this section, the voltage rise time is fixed to 0.5 ns and we study the influence of the value of the voltage plateau on the discharge dynamics and characteristics until it reaches the cathode plane. For applied voltages between 40 and 60 kV, Table 1 gives the values of several characteristics of the discharge dynamics: the ignition time (ns), the applied voltage at ignition (kV), the maximal and minimal values of $E_{x,max}$ (kV cm^{-1}) during the ionization front propagation in the gap, the connection time of the discharge to the plane (ns), the value of $E_{x,max}$ (kV cm^{-1}) at the plane at the connection time, the average propagation velocity of the discharge front in the gap (mm ns^{-1}), the voltage time rate (kV ns^{-1}) and the average electric field in the gap (kV cm^{-1}). The average propagation velocity of the discharge front in the gap is calculated by dividing the gap size by the difference between the connection time of the discharge to the plane and the ignition time, the voltage time rate is obtained by dividing the value of the voltage plateau by the rise time and the average electric field in the gap is obtained by dividing the value of the voltage plateau by the gap length.
First, surprisingly, Table 1 shows that the ignition time decreases of only 12% from 0.17 to 0.15 ns as the value of the voltage plateau increases by 50% from 40 to 60 kV. In the studied conditions, the voltage rise time is the same for all voltages, then the ignition voltage will depend on the value of the voltage plateau. Table 1 shows that the ignition voltage increases of 20% from 14.5 to 17.4 kV as the value of the voltage plateau increases from 40 to 60 kV. Conversely, as expected, the connection time strongly depends on the value of the voltage plateau. It decreases by 62% from 5.38 to 2.03 ns s the value of the voltage plateau increases by 50% from 40 to 60 kV. For applied voltages of $40, 50$ and 60 kV, Figure 4 shows cross-sectional views of the absolute value of the electric field and electron density at the connection time at the cathode, i.e. at $t = 5.38$, 3.04 and 2.03 ns, respectively. For all applied voltages, a conical discharge structure is obtained at the connection time with a maximal radius of the discharge of about 8 mm for all voltages.

These results suggest that in experiments with pulsed voltages as in Brisset (2019); Chng et al. (2019); Brisset et al. (2019), the observed discharge structure will strongly depend on the ratio between the connection time of the discharge and the voltage pulse duration. If this ratio is less than 1, the pulse duration is too short for the ionization front to cross the gap and then the plasma discharge remains located only close to the pin electrode with a rather spherical shape. If this ratio is around 1, the ionization wave has just the time to cross the gap, and the conical shape of the discharge connecting both electrodes will be observed. Finally, if this ratio is larger than 1, the discharge connecting both electrodes may heat the gas and then the transition to a spark may occur.

Applied voltage (kV)	40	45	50	55	60
Ignition time (ns)	0.17	0.16	0.15	0.15	0.15
Ignition voltage (kV)	14.5	14.6	14.4	15.8	17.4
Maximal value of $E_{x,max}$ (kV cm^{-1})	829	849	849	870	887
Minimal value of $E_{x,max}$ (kV cm^{-1})	80	88	96	104	111
Connection time to the plane (ns)	5.38	3.95	3.04	2.45	2.03
$E_{x,max}$ at connection time (kV cm^{-1})	205	211	228	215	233
Average front propagation velocity (mm ns^{-1})	3.1	4.2	5.5	7.0	8.5
Voltage time rate (kV ns^{-1})	80	90	100	110	120
Average electric field (kV cm^{-1})	25	28.1	31.2	34.4	37.5

Table 1. Characteristics of the discharges obtained for applied voltages ranging from 40 to 60 kV, with a rise time of 0.5 ns.

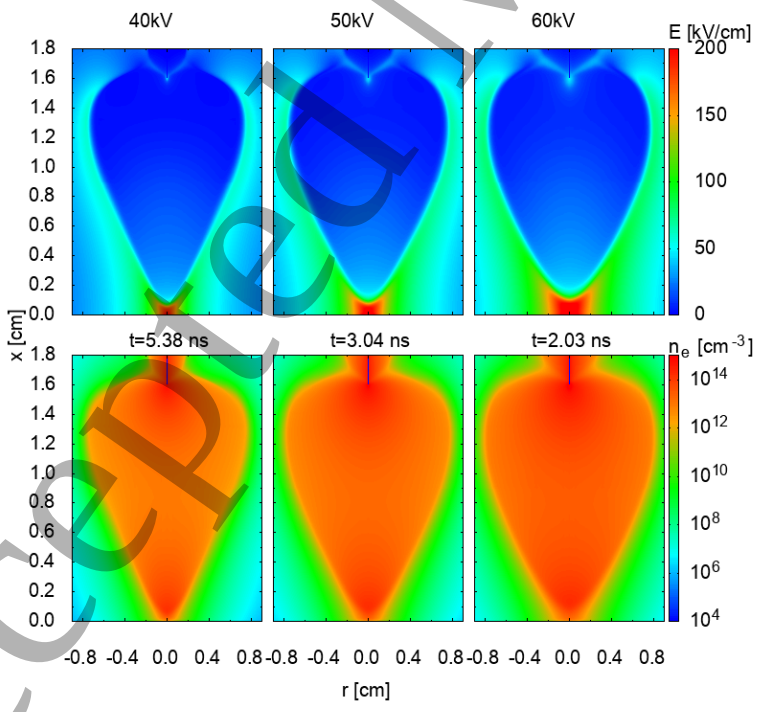

Figure 4. For applied voltages of 40, 50 and 60 kV and a rise time of 0.5 ns, cross-sectional views of the absolute value of the electric field and electron density at the connection time at the cathode, i.e. at $t = 5.38$, 3.04 and 2.03 ns, respectively.

Figure 5 shows the time evolution of $E_{x,max}$, the maximal electric field on the symmetry

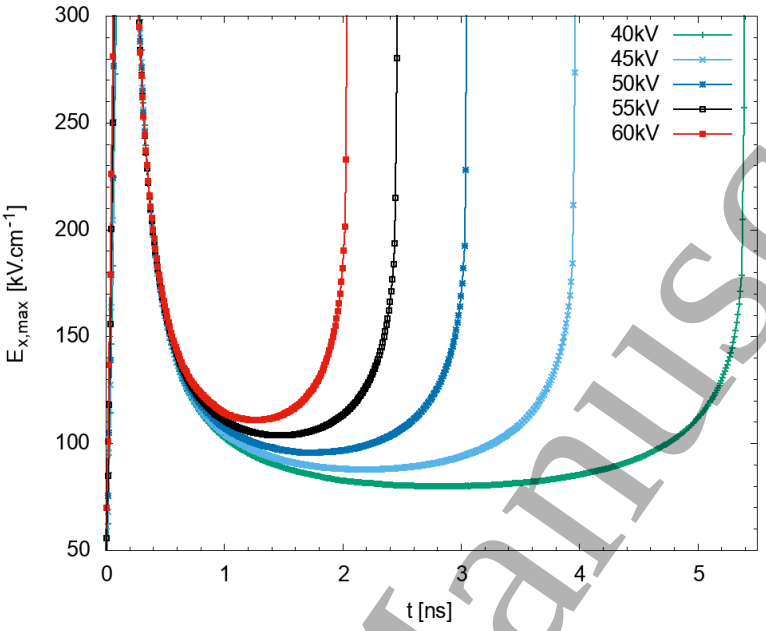

Figure 5. For applied voltages of 40 to 60 kV and a rise time of 0.5 ns, time evolution of $E_{x,max}$, the maximal value of the electric field on the symmetry axis of the discharge until it reaches the plane cathode.

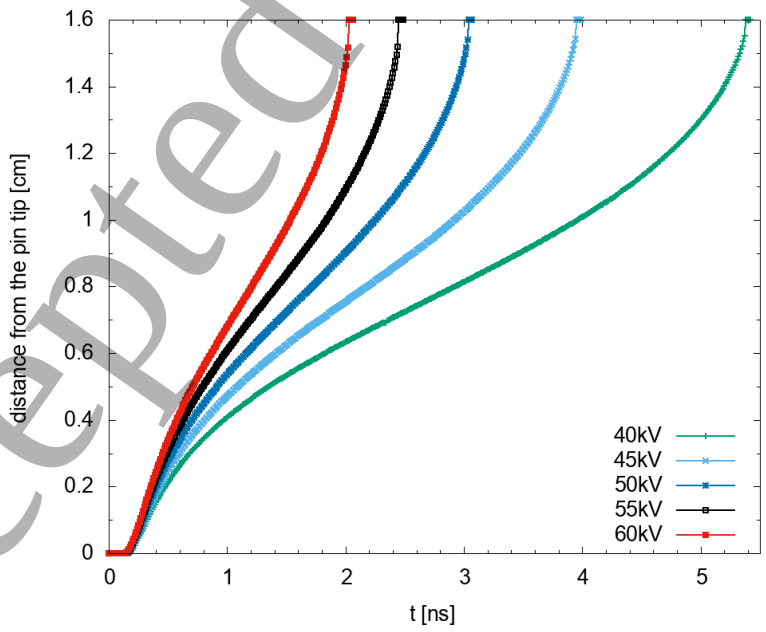

Figure 6. For applied voltages of 40 to 60 kV and a rise time of 0.5 ns, axial position of $E_{x,max}$.

axis of the discharge until it reaches the plane cathode for applied voltages between

40 and 60 kV. For all voltages, we note that, first, $E_{x,max}$ increases and decreases very rapidly and takes values higher than 240 kV cm^{-1} during less than 0.4 ns. For t$>$ 0.4 ns, $E_{x,max}$ first decreases as the discharge front propagates axially and increases again as the discharge front gets closer to the plane cathode. The minimal value of $E_{x,max}$ is obtained in all cases when the discharge front is around the middle of the gap and its value decreases from to 111 to 80 kV cm^{-1} as the applied voltage decreases from 60 to 40 kV. We note that the extent of the region with the lowest values of $E_{x,max}$ increases when the applied voltage decreases from 60 to 40 kV. To study more in detail the dynamics of propagation of the ionization front, Figure 6 shows the time evolution of the axial position of $E_{x,max}$ until it reaches the plane cathode. As discussed in Table 1, the ignition times for all studied voltages are very close and around 0.16 ns and Figure 6 shows that the discharge starts propagating from the pin to the plane at around $t = 0.2$ ns for all studied voltages in the range 40 to 60 kV. For $t > 0.2$ ns, we note that the propagation velocity of the ionization front varies during the early times of the propagation, then is almost constant and then increases as the discharge approaches the cathode. Table 1 shows that the average propagation velocity of the ionization front increases from 3.1 to 8.5 mm ns^{-1} as the applied voltage increases from 40 to 60 kV, which is in rather good agreement with experiments (Brisset; 2019).

.

3.3. For an applied voltage of 55 kV, influence of the voltage rise time on the discharge dynamics and characteristics

In this section, we study the influence of the voltage rise time, in considering the three voltage shapes shown on Figure 1, i.e. with 0.5 and 1.5 ns voltage rise times and a DC voltage with a voltage plateau at 55 kV. Figures 7 and 8 show the time evolutions of $E_{x,max}$ and of the axial position of $E_{x,max}$ until the discharge front reaches the plane cathode. For the three studied cases, Table 2 gathers the values of several key quantities of the discharge dynamics. First, in Table 2 and Figures 7 and 8, we note, as expected, that the discharge starts to propagate as early as 0.01 ns for a DC voltage and the ignition time increases from 0.15 ns to 0.25 ns as the voltage rise time increases from 0.5 to 1.5 ns. The voltage at ignition is the highest for the DC voltage and decreases from 15.8 to 9.2 kV as the voltage rise time increases from 0.5 to 1.5 ns. For $t \leq 0.5$ ns, for a DC voltage, the maximal value of $E_{x,max}$ is at $t = 0$ ns (3 MV cm^{-1} due to the sharp pin electrode) and then decreases very rapidly whereas for an applied voltage with voltage rise times of 0.5 and 1.5 ns, for $t \leq 0.5$ ns, $E_{x,max}$ first increases and then decreases. As shown in Table 2, the maximal value of $E_{x,max}$ decreases from 870 to 553 kV cm^{-1} as the voltage rise time increases from 0.5 to 1.5 ns. We note that the increase and decrease of $E_{x,max}$ occurs slightly earlier for a rise time of 0.5 ns than for 1.5 ns.

For t$>$ 0.5 ns, for all cases, $E_{x,max}$ decreases as the discharge propagates axially and increases again as the discharge gets closer to the plane cathode. The minimal value of $E_{x,max}$ is obtained for all three cases when the discharge front is around the middle of

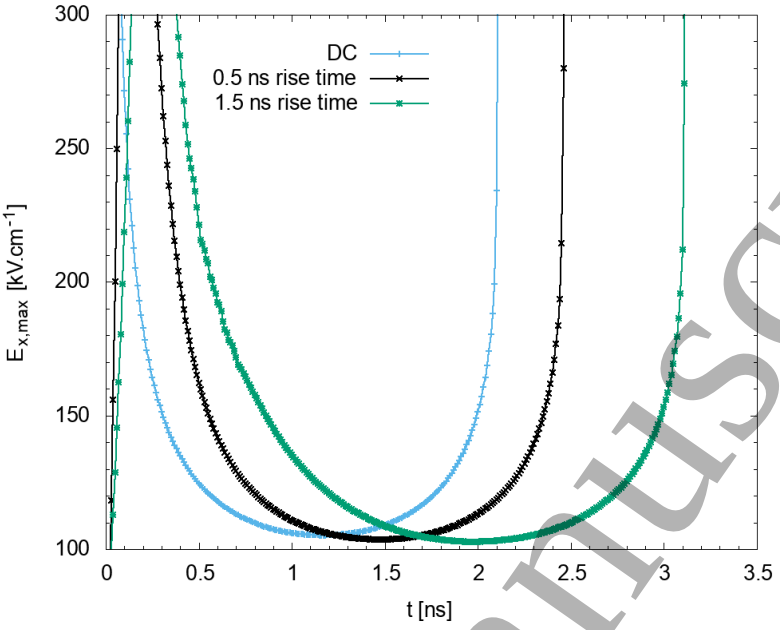

Figure 7. For a DC applied voltage and voltages with rise times of 0.5 and 1.5 ns and a voltage plateau of 55 kV: time evolution of $E_{x,max}$, the maximal value of the electric field on the symmetry axis of the discharge until it reaches the plane cathode.

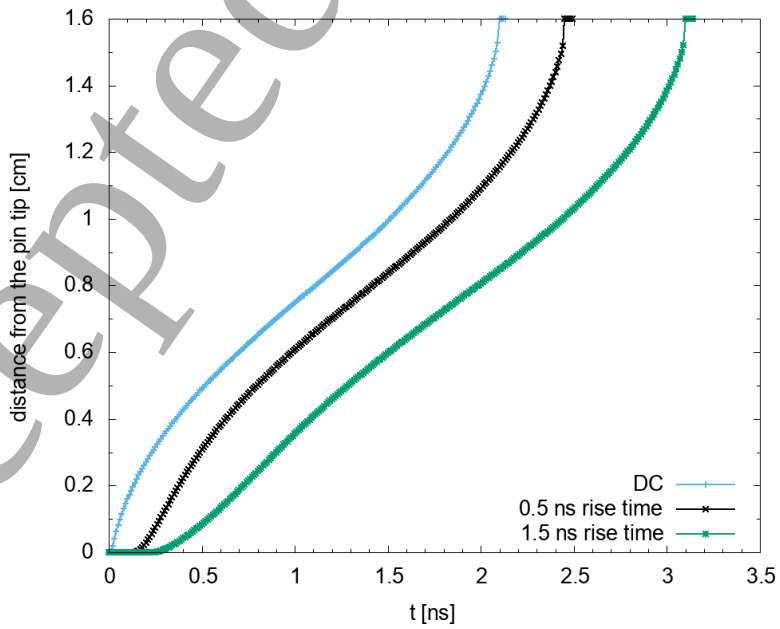

Figure 8. For a DC applied voltage and voltages with rise times of 0.5 and 1.5 ns and a voltage plateau of 55 kV: axial position of $E_{x,max}$.

Voltage plateau of 55 kV	DC	0.5 ns rise time	1.5 ns rise time
Ignition time (ns)	0.01	0.15	0.25
Ignition voltage (kV)	55	15.8	9.2
Maximal value of $E_{x,max}$ (kV cm^{-1})	3543	870	553
Minimal value of $E_{x,max}$ (kV cm^{-1})	105	104	103
Connection time to the plane (ns)	2.10	2.45	3.10
$E_{x,max}$ at connection time (kV cm^{-1})	234	215	212
Average front propagation velocity (mm ns^{-1})	7.7	7.0	5.6
Voltage time rate (kV ns^{-1})	–	110	36.3
Average electric field (kV cm^{-1})	34.4	34.4	34.4

Table 2. Influence of the shape of the applied voltage for a voltage plateau of 55 kV.

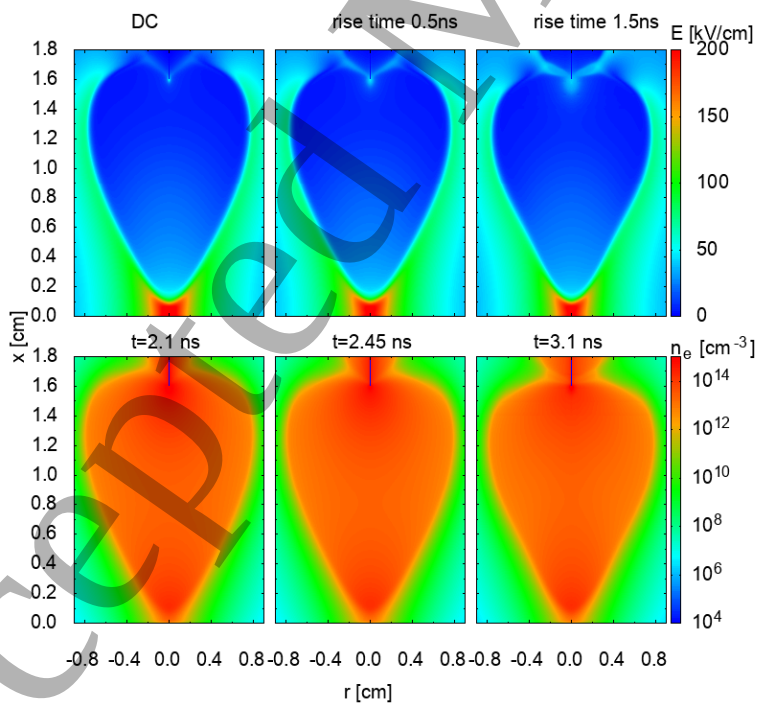

Figure 9. For a DC applied voltage and voltages with rise times of 0.5 and 1.5 ns and a voltage plateau of 55 kV: cross-sectional views of the absolute value of the electric field and electron density at the connection time at the cathode, i.e. at $t = 2.1$, 2.45 and 3.1 ns, respectively.

the gap and its value is about 104 kV cm^{-1}.

For the three cases, Figure 9 shows cross-sectional views of the absolute value of the electric field and electron density at the connection time at the cathode, i.e. at $t = 2.1$ ns for the DC voltage and $t = 2.45$ and 3.1 ns for voltage rise times of 0.5 and 1.5 ns, respectively. As expected, we note that the shortest connection time is obtained for the DC voltage and that the connection time increases as the voltage rise time increases. Figure 9 shows that at the time of connection, in the three conditions, the discharge has a very similar conical structure, with in particular the same maximal radius of about 8 mm.

Figure 8 shows that for all studied cases, the propagation velocity of the ionization front varies during the early times of the propagation, then is almost constant and then increases as the discharge approaches the cathode. Table 2 shows that the average propagation velocity of the ionization front decreases from 7.7 to 5.6 mm ns^{-1} as the voltage goes from a DC voltage to a voltage applied with a rise time of 1.5 ns.

3.4. For an applied voltage of 55 kV and a rise time of 0.5 ns, time evolution of the electric field for several points in the gap

To compare qualitatively with recent electric field measurements (Brisset; 2019; Chng et al.; 2019), in this section, we study for the reference case of an applied voltage of 55 kV and a rise time of 0.5 ns, the time evolution of the axial electric field E_x on the symmetry axis of the discharge for different axial positions in the interelectrode gap. We define d as the axial distance from the tip of the pin electrode and we study results at $d = 2, 5, 8, 11$ and 14 mm. For $t < 2.45$ ns (i.e. before the connection time at the cathode) Figure 10 shows that for all positions, a peak of electric field is observed with a time shift showing the axial propagation of the ionization front from the pin to the plane, in agreement with experiments (Brisset; 2019). As already shown on Figure 5, the value of $\mathrm{E}_{x,max}$ depends on the studied axial position. Figure 10(a) also shows that the shape of the peak of electric field depends on the studied axial position. We note that the width of the peak of electric field increases and the value of $\mathrm{E}_{x,max}$ decreases as the studied point moves from $d = 2$ mm to $d = 8$ mm. Then as the studied point gets closer to the cathode from $d = 8$ mm to $d = 14$ mm, the width of the peak of electric field decreases and the value of $\mathrm{E}_{x,max}$ increases. Figure 11 compares the time evolution of E_x, the electric field on the symmetry axis of the discharge, at $d = 2$ and 14 mm with the time evolution of the Laplacian electric field at the same positions. The Laplacian electric field at $d = 5$ mm is also shown. The Laplacian electric field is obtained by solving Poisson's equation for same electrode geometry and applied voltage at a given time, but with volume charge densities set to zero. As expected, during the voltage rise time of 0.5 ns, the Laplacian electric field increases at all studied points. Due to the pin-to-plane geometry used, the Laplacian electric field is highly non-uniform in the gap with higher values close to the pin electrode. For $t \geq 0.5$ ns, when the voltage plateau is reached, the Laplacian electric field remains constant at all studied points.

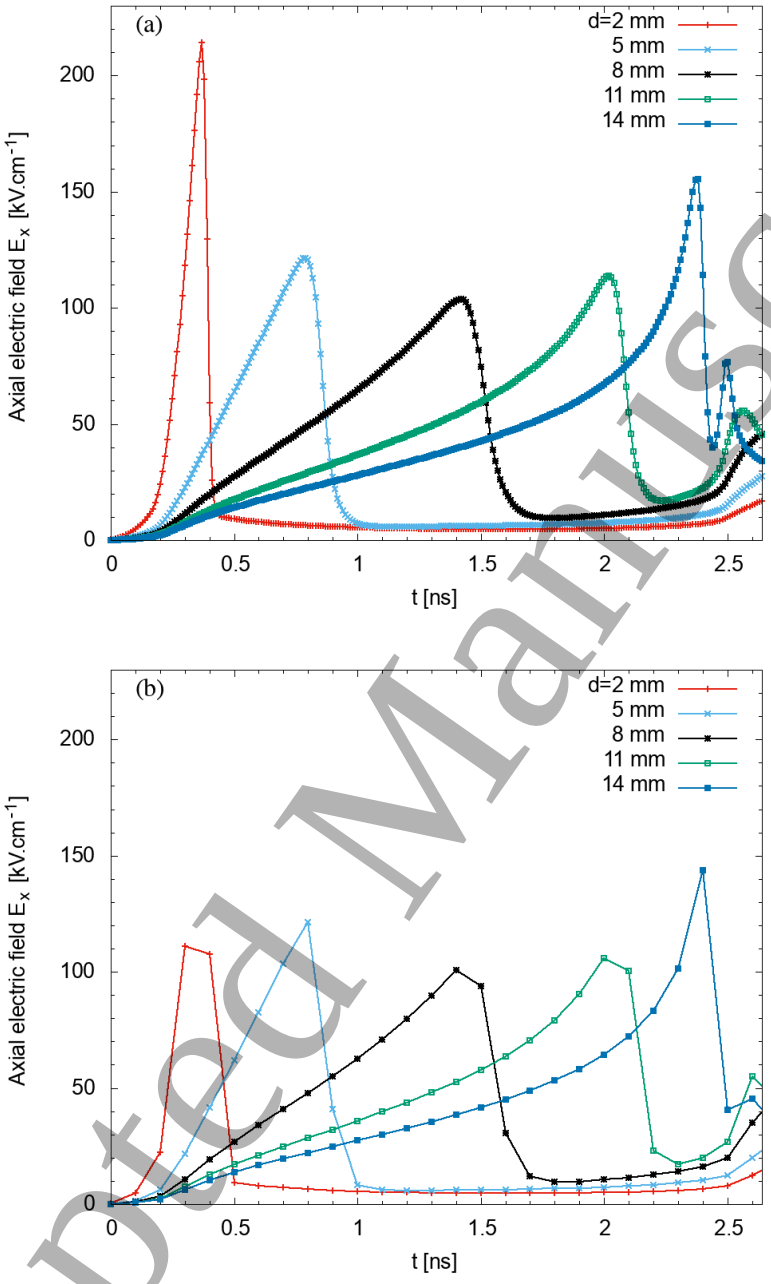

Figure 10. For an applied voltage of 55 kV and a rise time of 0.5 ns : time evolutions of the axial electric field E_x on the symmetry axis of the discharge at different distances d from the pin electrode. (a) : with a time sampling of 10 ps. (b) : with a time sampling of 100 ps.

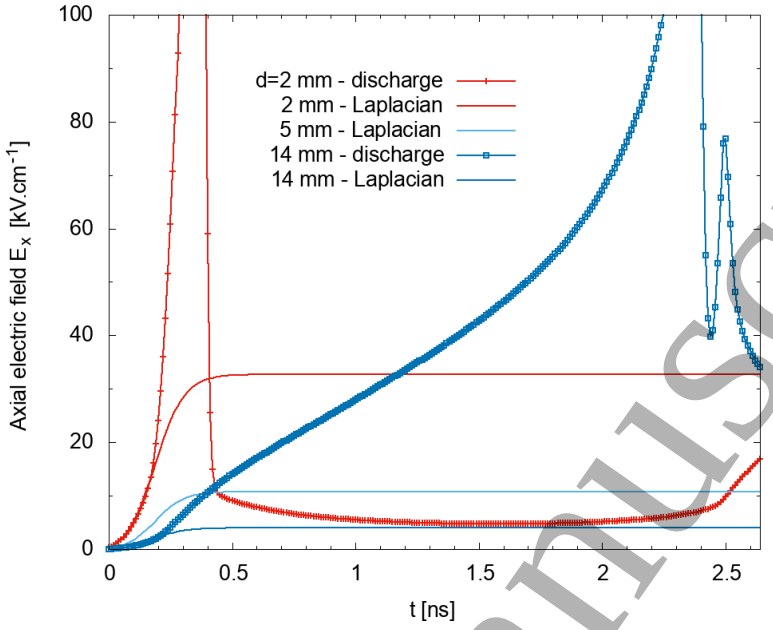

Figure 11. For an applied voltage of 55 kV and a rise time of 0.5 ns : time evolution of the axial electric field E_x on the symmetry axis of the discharge at $d = 2$ and 14 mm and time evolution of the axial Laplacian electric field on the symmetry axis at $d = 2$, 5 and 14 mm.

It is interesting to note that at $d = 2$ mm, the Laplacian electric field for the voltage plateau (i.e. $t \geq 0.5$ ns) is 32.7 kV cm^{-1}, higher than the breakdown electric field whereas the values for $d = 5$ and 14 mm are only of 10.8 and 4 kV cm^{-1}, respectively. We note that initially, the evolution of the electric field in the discharge simulation is the same as the Laplacian electric field but, as early as $t = 0.18$ and 0.21 ns for $d = 2$ and 14 mm, respectively, the electric field in the discharge simulation becomes higher than the Laplacian electric field. We note that the slope of the electric field increase in the discharge simulation is very sharp for the studied point $d = 2$ mm, close to the tip and much smoother for $d = 14$ mm. This increase of the electric field ahead of the ionization front, also observed in experiments (Chng et al.; 2019), is due to the redistribution of the electric field in the gap as the ionization front propagates. It is interesting to note that due both to the geometry (sharp point in a pin to plane geometry) and the high applied voltage, the electric field ahead of the discharge front becomes higher than 30 kV cm^{-1} as early as $t = 0.22$ and 1.07 ns, at $d = 2$ and 14 mm, respectively. After the peak, at all studied points, the decrease of electric field is much faster than its increase as observed in experiments (Chng et al.; 2019). In Figure 10(a), we note that after the peak, the electric field goes down to a minimal value which increases as the studied point moves from the anode to the cathode. It is 4.75 kV cm^{-1} for $d = 2$mm, 9.5 kV cm^{-1} for $d = 8$mm and 40 kV cm^{-1} for $d = 14$mm.

For $t \geq 2.45$ ns, i.e. after the connection of the discharge at the plane, Figure 10 shows a sharp peak of electric field occurring first at $t = 2.49$ ns at $d = 14$ mm with a maximal

value of 77 kV cm^{-1}, followed by a lower and wider peak at $d = 11$ mm with a maximal value of 56 kV cm^{-1} at t=2.56 ns. These two peaks correspond to the fast propagation of a return wave from the cathode towards the anode. We note that for points closer to the pin electrode (i.e. for $d \leq 8$ mm on Figure 10), only an increase of electric field is observed, and this increase is larger for points which are closer to the cathode. This means that a fast return wave starts propagating from the cathode but rapidly slows down. At $t = 2.6$ ns, we note on Figure 3 that the maximum of electric field due to the return wave is located at $x = 0.55$ cm and is of 53 kV cm^{-1}. As also observed on Figure 3, Figure 10 shows that rapidly after the connection, the electric field is not uniform in the gap and is in many points of the gap higher than the breakdown field in air at atmospheric pressure and also higher than the average electric field of 34.4 kV cm^{-1} simply calculated by dividing the applied voltage by the gap distance.

Instantaneous results in Figure 10(a) and 11 are shown with a time sampling of 10 ps. In the recent experimental works (Brisset; 2019; Chng et al.; 2019), the shortest time resolution for electric field measurements on the discharge axis is estimated to be 150 ps. Figure 10 (a) and (b) compares instantaneous results obtained with a time sampling of 10 and 100 ps. We note that for our studied conditions, a time resolution of 100 ps would allow to capture the dynamics and maximal values of electric field during the diffuse ionization wave propagation for a studied position close to the middle of the discharge gap. However, for studied points closer to both electrodes, a time resolution of the order of 10 ps would be required to capture the dynamics and maximal values of electric field. Figure 10 also shows that with a time resolution of 100 ps, the redistribution of the electric field after the connection can be observed, but only a time resolution of about 10 ps allows to follow accurately its fast dynamics.

4. Conclusions

In this paper, the dynamics of a diffuse nanosecond positive ionization wave generated in a pin-to-plane geometry in atmospheric pressure air is simulated using a 2D axisymmetric drift-diffusion fluid model. For a 16 mm gap and a pin electrode with a radius of curvature of 100 μm, the plateau of the applied voltage is varied between 40 and 60 kV and the voltage rise time is varied between 0.5 and 1.5 ns or a DC voltage is applied. In this work, we have focused on discharge characteristics that could be compared with experiments: propagation velocity, maximal discharge radius and electric field on the discharge axis. In all studied cases, we show that the discharge has a large conical shape with a maximal radius of about 8 mm as it connects to the grounded plane, which is in rather good agreement with experiments (Brisset; 2019; Chng et al.; 2019) The discharge ignition time and the voltage at the ignition time are shown to depend mostly on the voltage rise time. The connection time, i.e. the time for the ionization wave to ignite, propagate in the gap and connect to the plane electrode are shown to strongly depend on both the value of the voltage plateau and

the voltage rise time. The connection time decreases by 62% from 5.38 to 2.03 ns as the value of the voltage plateau increases by 50% from 40 to 60 kV for a rise time of 0.5 ns. As expected, for a value of voltage plateau of 55 kV, the shortest connection time is obtained for DC voltages, and the connection time increases as the voltage rise time increases. These results suggest that in experiments with pulsed voltages, the observed discharge structure will strongly depend on the ratio between the connection time of the discharge and the voltage pulse duration. If this ratio is less than 1, the pulse duration is too short for the ionization front to cross the gap and then the plasma discharge remains located only close to the pin electrode with a rather spherical shape. If this ratio is around 1, the ionization wave has just the time to cross the gap, and the conical shape of the discharge connecting both electrodes will be observed.

For all studied cases, we show that the propagation velocity of the ionization front varies during the early times of the propagation, then is almost constant and then increases as the discharge approaches the cathode. For a rise time of 0.5 ns, the average propagation velocity of the ionization front increases from 3.1 to 8.5 mm ns^{-1} as the applied voltage increases from 40 to 60 kV. For a voltage plateau of 55 kV, the average propagation velocity of the ionization front decreases from 7.7 to 5.6 mm ns^{-1} as the voltage goes from a DC voltage to a voltage rise time of 1.5 ns. These values are in rather good agreement with experiments (Brisset; 2019).

The time evolution of the maximum value of the electric field on the discharge axis $E_{x,max}$ at different locations of the gap is studied for applied voltages between 40 and 60 kV with a rise time of 0.5 ns. For all cases, $E_{x,max}$ is shown first to increase and decrease very rapidly and takes values higher than 240 kV cm^{-1} during less than 0.4 ns. For t$>$ 0.4 ns, as the discharge propagates axially, $E_{x,max}$ first decreases and increases again as the discharge gets closer to the plane cathode. In all studied cases, the minimal value of $E_{x,max}$ is obtained when the discharge front is around the middle of the gap and its value decreases from to 111 to 80 kV cm^{-1} as the applied voltage decreases from 60 to 40 kV. The time evolution of the electric field on the symmetry axis at different locations of the gap for 55 kV with a rise time of 0.5 ns is qualitatively compared with experiments. At each studied location, an increase and decrease of the electric field is observed as the ionization front, propagating from the pin to the plane, passes the studied location, in accordance with experimental observations (Brisset; 2019). For all studied points, the increase of electric field is shown to be slower than its decrease, as observed in experiments (Chng et al.; 2019). The shape of the peak of electric field is shown to depend on the studied axial position. The width of the peak of electric field increases and the maximum value of the electric field decreases as the studied point moves from the vicinity of the point electrode to the middle of the gap. Then as the studied point gets closer to the cathode, the width of the peak of electric field decreases and the maximum value of the electric field increases. As observed in experiments (Chng et al.; 2019), after the discharge ignition, the electric field ahead of the ionization front becomes rapidly higher than the Laplacian electric field. Simulations show that this is due to the redistribution of the electric field in the gap as the ionization front propagates. After the

peak, the electric field goes down to a minimal value which increases as the studied point moves from the anode to the cathode. After the connection of the discharge at the plane, a very fast redistribution of electric field in the conductive channel is observed with a fast wave propagating from the cathode towards the anode. Just after the connection, The electric field is shown to be non uniform in the gap and may be in many points of the gap higher than the breakdown field in air at atmospheric pressure.
Finally, for the reference case with 55 kV and a rise time of 0.5 ns, we show that a time resolution of 100 ps would allow to capture the dynamics and maximum values of electric field for a studied position close to the middle of the discharge gap. However, only a time resolution of about 10 ps allows to follow accurately the fast dynamics of the electric field during the propagation of the ionization wave for studied points close to electrodes or during the redistribution of the electric after the connection of the ionization wave at the cathode.

Acknowledgments

The authors are thankful to Drs Tat Loon Chng, Svetlana Starikovskaia, Alexandra Brisset, Pierre Tardiveau, Eric Robert and Jean-Michel Pouvesle for discussions on the experimental study of nanosecond diffuse discharges in air at atmospheric pressure. ZB acknowledges support by project LM2018097 funded by the Ministry of Education, Youth and Sports of the Czech Republic. Simulations presented in this work have been performed thanks to the computational resources of the cluster Hopper at Ecole Polytechnique.

References

Babaeva, N. Y. and Naidis, G. V. (1996). Two-dimensional modelling of positive streamer dynamics in non-uniform electric fields in air, *Journal of Physics D: Applied Physics* **29**(9): 2423–2431.
URL: *https://doi.org/10.1088/0022-3727/29/9/029*

Babaeva, N. Y. and Naidis, G. V. (2016a). Modeling of streamer dynamics in atmospheric-pressure air: Influence of rise time of applied voltage pulse on streamer parameters, *IEEE Transactions on Plasma Science* **44**(6): 899–902.
URL: *https://doi.org/10.1109/TPS.2016.2553081*

Babaeva, N. Y. and Naidis, G. V. (2016b). Simulation of subnanosecond streamers in atmospheric-pressure air: Effects of polarity of applied voltage pulse, *Physics of Plasmas* **23**(8): 083527.
URL: *https://doi.org/10.1063/1.4961925*

Bourdon, A., Pasko, V. P., Liu, N., Célestin, S., Ségur, P. and Marode, E. (2007). Efficient models for photoionization produced by non-thermal gas discharges in air based on radiative transfer and the helmholtz equations, *Plasma Sources Science and*

Technology **16**(3): 656–678.
URL: *https://doi.org/10.1088/0963-0252/16/3/026*

Briels, T. M. P., Kos, J., van Veldhuizen, E. M. and Ebert, U. (2006). Circuit dependence of the diameter of pulsed positive streamers in air, *Journal of Physics D: Applied Physics* **39**(24): 5201–5210.
URL: *https://doi.org/10.1088/0022-3727/39/24/016*

Briels, T. M. P., Kos, J., Winands, G. J. J., van Veldhuizen, E. M. and Ebert, U. (2008). Positive and negative streamers in ambient air: measuring diameter, velocity and dissipated energy, *Journal of Physics D: Applied Physics* **41**(23): 234004.
URL: *https://doi.org/10.1088/0022-3727/41/23/234004*

Brisset, A. (2019). *Physique des décharges nanosecondes diffuses générées sous champs électriques extrêmes*, PhD thesis, Université Paris-Saclay.
URL: *https://tel.archives-ouvertes.fr/tel-02466313*

Brisset, A., Gazeli, K., Magne, L., Pasquiers, S., Jeanney, P., Marode, E. and Tardiveau, P. (2019). Modification of the electric field distribution in a diffuse streamer-induced discharge under extreme overvoltage, *Plasma Sources Science and Technology* **28**(5): 055016.
URL: *https://doi.org/10.1088/1361-6595/ab1989*

Celestin, S., Bonaventura, Z., Zeghondy, B., Bourdon, A. and Ségur, P. (2009). The use of the ghost fluid method for Poisson's equation to simulate streamer propagation in point-to-plane and point-to-point geometries, *Journal of Physics D: Applied Physics* **42**(6): 065203.
URL: *https://doi.org/10.1088/0022-3727/42/6/065203*

Chng, T. L., Brisset, A., Jeanney, P., Starikovskaia, S. M., Adamovich, I. V. and Tardiveau, P. (2019). Electric field evolution in a diffuse ionization wave nanosecond pulse discharge in atmospheric pressure air, *Plasma Sources Science and Technology* **28**(9): 09LT02.
URL: *https://doi.org/10.1088/1361-6595/ab3cfc*

Dubois, D., Merbahi, N., Eichwald, O., Yousfi, M. and Benhenni, M. (2007). Electrical analysis of positive corona discharge in air and N_2, O_2, and CO_2 mixtures, *Journal of Applied Physics* **101**(5): 053304.
URL: *https://doi.org/10.1063/1.2464191*

Eichwald, O., Ducasse, O., Dubois, D., Abahazem, A., Merbahi, N., Benhenni, M. and Yousfi, M. (2008). Experimental analysis and modelling of positive streamer in air: towards an estimation of O and N radical production, *Journal of Physics D: Applied Physics* **41**(23): 234002.
URL: *https://doi.org/10.1088/0022-3727/41/23/234002*

Jánský, J., Tholin, F., Bonaventura, Z. and Bourdon, A. (2010). Simulation of the discharge propagation in a capillary tube in air at atmospheric pressure, *Journal of Physics D: Applied Physics* **43**: 395201.
URL: *http://stacks.iop.org/0022-3727/43/i=39/a=395201*

Komuro, A., Ono, R. and Oda, T. (2013). Effects of pulse voltage rise rate on velocity, diameter and radical production of an atmospheric-pressure streamer discharge, *Plasma Sources Science and Technology* **22**(4): 045002.
URL: *https://doi.org/10.1088/0963-0252/22/4/045002*

Kulikovsky, A. A. (1997). Positive streamer between parallel plate electrodes in atmospheric pressure air, *Journal of Physics D: Applied Physics* **30**: 441–450.
URL: *http://stacks.iop.org/0.1088/0022-3727/30/3/017*

Kulikovsky, A. A. (1998). Positive streamer in a weak field in air : A moving avalanche-to-streamer transition, *Physical Review E* **57**: 7066–7074.
URL: *http://stacks.iop.org/10.1103/PhysRevE.57.7066*

Kunhardt, E. E., Tzeng, Y. and Boeuf, J. P. (1986). Stochastic development of an electron avalanche, *Physical Review A* **34**: 440–449.
URL: *https://link.aps.org/doi/10.1103/PhysRevA.34.440*

Liu, N., Célestin, S., Bourdon, A., Pasko, V. P., Ségur, P. and Marode, E. (2007). Application of photoionization models based on radiative transfer and the helmholtz equations to studies of streamers in weak electric fields, *Applied Physics Letters* **91**(21): 211501.
URL: *http://link.aip.org/link/?APL/91/211501/1*

Marode, E. (1975a). The mechanism of spark breakdown in air at atmospheric pressure between a positive point and a plane. i. experimental: Nature of the streamer track, *Journal of Applied Physics* **46**(5): 2005–2015.
URL: *https://doi.org/10.1063/1.321882*

Marode, E. (1975b). The mechanism of spark breakdown in air at atmospheric pressure between a positive point and plane. ii. theoretical: Computer simulation of the streamer track, *Journal of Applied Physics* **46**(5): 2016–2020.
URL: *https://doi.org/10.1063/1.321814*

Marode, E., Dessante, P. and Tardiveau, P. (2016). 2d positive streamer modelling in NTP air under extreme pulse fronts. what about runaway electrons?, *Plasma Sources Science and Technology* **25**(6): 064004.
URL: *https://doi.org/10.1088/0963-0252/25/6/064004*

Marode, E., Djermoune, D., Dessante, P., Deniset, C., Ségur, P., Bastien, F., Bourdon, A. and Laux, C. (2009). Physics and applications of atmospheric non-thermal air plasma with reference to environment, *Plasma Physics and Controlled Fusion* **51**(12): 124002.
URL: *https://doi.org/10.1088/0741-3335/51/12/124002*

Morrow, R. and Lowke, J. J. (1997). Streamer propagation in air, *Journal of Physics D: Applied Physics* **30**: 614–627.
URL: *https://doi.org/10.1088/0022-3727/30/4/017*

Moss, G. D., Pasko, V. P., Liu, N. and Veronis, G. (2006). Monte carlo model for analysis of thermal runaway electrons in streamer tips in transient luminous events and

streamer zones of lightning leaders, *Journal of Geophysical Research: Space Physics* **111**(A2).
URL: *https://agupubs.onlinelibrary.wiley.com/doi/abs/10.1029/2005JA011350*

Naidis, G. V., Tarasenko, V. F., Babaeva, N. Y. and Lomaev, M. I. (2018). Subnanosecond breakdown in high-pressure gases, *Plasma Sources Science and Technology* **27**(1): 013001.
URL: *https://doi.org/10.1088/1361-6595/aaa072*

Nijdam, S. (2011). *Experimental investigations on the physics of streamers*, PhD thesis, Eindhoven University of Technology.

Ono, R. and Komuro, A. (2019). Generation of the single-filament pulsed positive streamer discharge in atmospheric-pressure air and its comparison with two-dimensional simulation, *Journal of Physics D: Applied Physics* **53**(3): 035202.
URL: *https://doi.org/10.1088/1361-6463/ab4e65*

Ono, R. and Oda, T. (2003). Formation and structure of primary and secondary streamers in positive pulsed corona discharge—effect of oxygen concentration and applied voltage, *Journal of Physics D: Applied Physics* **36**(16): 1952–1958.
URL: *https://doi.org/10.1088/0022-3727/36/16/306*

Pancheshnyi, S., Nudnova, M. and Starikovskii, A. (2005). Development of a cathode-directed streamer discharge in air at different pressures : Experiment and comparison with direct numerical simulation, *Physical Review E* **71**: 016407–1 – 016407–11.
URL: *https://link.aps.org/doi/10.1103/PhysRevE.71.016407*

Pancheshnyi, S. V., Starikovskaia, S. M. and Starikovskii, A. Y. (2000). Role of photoionization processes in propagation of cathode-directed streamer, *Journal of Physics D: Applied Physics* **34**(1): 105–115.
URL: *https://doi.org/10.1088/0022-3727/34/1/317*

Pechereau, F. (2013). *Numerical simulation of the interaction of a plasma discharge at atmospheric pressure with dielectric surfaces*, PhD thesis, Ecole Centrale Paris, France.
URL: *https://tel.archives-ouvertes.fr/tel-00978523*

Pechereau, F., Le Delliou, P., Jnsk, J., Tardiveau, P., Pasquiers, S. and Bourdon, A. (2014). Large conical discharge structure of an air discharge at atmospheric pressure in a point-to-plane geometry, *IEEE Transactions on Plasma Science* **42**(10): 2346–2347.
URL: *https://doi.org/10.1109/TPS.2014.2309981*

Sigmond, R. S. (1984). The residual streamer channel: Return strokes and secondary streamers, *Journal of Applied Physics* **56**(5): 1355–1370.
URL: *https://doi.org/10.1063/1.334126*

Tarasenko, V. (2020). Runaway electrons in diffuse gas discharges, *Plasma Sources Science and Technology* **29**(3): 034001.
URL: *https://doi.org/10.1088/1361-6595/ab5c57*

Tardiveau, P., Magne, L., Marode, E., Ouaras, K., Jeanney, P. and Bournonville, B. (2016). Sub-nanosecond time resolved light emission study for diffuse discharges in air under steep high voltage pulses, *Plasma Sources Science and Technology* **25**(5): 054005.
URL: *https://doi.org/10.1088/0963-0252/25/5/054005*

Tardiveau, P., Marode, E. and Agneray, A. (2002). Tracking an individual streamer branch among others in a pulsed induced discharge, *Journal of Physics D: Applied Physics* **35**(21): 2823–2829.
URL: *https://doi.org/10.1088/22-3727/35/21/319*

Tardiveau, P., Moreau, N., Bentaleb, S., Postel, C. and Pasquiers, S. (2009). Diffuse mode and diffuse-to-filamentary transition in a high pressure nanosecond scale corona discharge under high voltage, *Journal of Physics D: Applied Physics* **42**(17): 175202.
URL: *https://doi.org/10.1088/0022-3727/42/17/175202*

Tardiveau, P., Moreau, N., Jorand, F., Postel, C., Pasquiers, S. and Vervisch, P. (2008). Nanosecond scale discharge dynamics in high pressure air, *IEEE Transactions on Plasma Science* **36**(4): 894–895.
URL: *https://doi.org/10.1109/TPS.2008.917770*

Teunissen, J. and Ebert, U. (2016). 3d PIC-MCC simulations of discharge inception around a sharp anode in nitrogen/oxygen mixtures, *Plasma Sources Science and Technology* **25**(4): 044005.
URL: *https://doi.org/10.1088/0963-0252/25/4/044005*

Tholin, F. (2012). *Numerical simulation of nanosecond repetitively pulsed discharges in air at atmospheric pressure: Application to plasma-assisted combustion*, PhD thesis, Ecole Centrale Paris, France.
URL: *https://tel.archives-ouvertes.fr/tel-00879856*

Xiong, Z., Robert, E., Sarron, V., Pouvesle, J.-M. and Kushner, M. J. (2012). Dynamics of ionization wave splitting and merging of atmospheric-pressure plasmas in branched dielectric tubes and channels, *Journal of Physics D: Applied Physics* **45**(27): 275201.
URL: *https://doi.org/10.1088/0022-3727/45/27/275201*

Yi, W. J. and Williams, P. F. (2002). Experimental study of streamers in pure N_2 and N_2/O_2 mixtures and a ≈13 cm gap, *Journal of Physics D: Applied Physics* **35**(3): 205–218.
URL: *https://doi.org/10.1088/0022-3727/35/3/308*